DEAP S-18

J. Mech. Phys. Solids, 1977, Vol. 25, pp. 81 to 97. Pergamon Press. Printed in Great Britain.

CRACK-TIP FIELDS IN STEADY CRACK-GROWTH WITH LINEAR STRAIN-HARDENING†

By J. C. AMAZIGO

Department of Mathematical Sciences,
Rensselaer Polytechnic Institute, Troy, New York 12181, U.S.A.

and J. W. HUTCHINSON

Division of Engineering and Applied Physics,
Harvard University, Cambridge, Massachusetts 02138, U.S.A.

(*Received 7th July* 1976)

SUMMARY

SINGULAR stress and strain fields are found at the tip of a crack growing steadily and quasi-statically into an elastic-plastic strain-hardening material. The material is characterized by J_2 flow theory together with a bilinear effective stress–strain curve. The cases of anti-plane shear, plane stress and plane strain are each considered. Numerical results are given for the order of the singularity, details of the stress and strain-rate fields, and the near-tip regions of plastic loading and elastic unloading.

1. INTRODUCTION

FOR STATIONARY cracks in a given mode of loading, strain-hardening plays the important role of producing *unique* stress and strain fields in the plastic zone near a crack tip. A single amplitude factor measures the intensity of these fields. Only through this factor do overall geometry and applied load influence near-tip behavior. In the present paper, analogous near-tip fields are determined for steady, quasi-static crack growth in strain-hardening, elastic-plastic materials characterized by J_2 flow theory and a bilinear effective stress–strain curve. The cases of anti-plane shear (Mode III), plane stress and plane strain (Mode I) are each treated. We start with the anti-plane shear analysis, since, of the three cases, it can be presented in most detail with least complication.

2. ANTI-PLANE SHEAR ANALYSIS

Let x_i be rectangular Cartesian coordinates travelling with the crack tip and with the x_3-axis lying along the crack edge as shown in Fig. 1. Non-zero stresses and strains are $\tau_\beta \equiv \sigma_{3\beta}$ and $\gamma_\beta \equiv 2\varepsilon_{3\beta}$ with $\beta = 1, 2$. Let

$$\tau = (\tau_1^2 + \tau_2^2)^{\frac{1}{2}} \tag{2.1}$$

† This work was supported in part by the Advanced Research Projects Agency under Contract F44620-75-C-0088, in part by the Air Force Office of Scientific Research under Grant AFOSR-73-2476, in part by the National Science Foundation under Grant MPS75-08328 with Rensselaer Polytechnic Institute, and by the Division of Engineering and Applied Physics, Harvard University.

be the effective shear stress. In a simple shearing history, the shear stress and strain are taken to be related by the bilinear stress–strain curve shown in Fig. 1. The small-strain generalization to multi-axial incremental behavior according to J_2 flow theory (Prandtl-Reuss theory) is

$$G_t\dot{\gamma}_\beta = \alpha\dot{t}_\beta + (1-\alpha)\tau^{-1}\tau_\beta\dot{\tau} \qquad \text{(plastic loading, } \dot{t} \geq 0\text{)}, \tag{2.2}$$

$$G_t\dot{\gamma}_\beta = \alpha\dot{t}_\beta \qquad \text{(elastic unloading, } \dot{t} < 0\text{)}, \tag{2.3}$$

where $\alpha = G_t/G$ and $(\cdot)$ denotes material differentiation with respect to any monotonically increasing quantity.

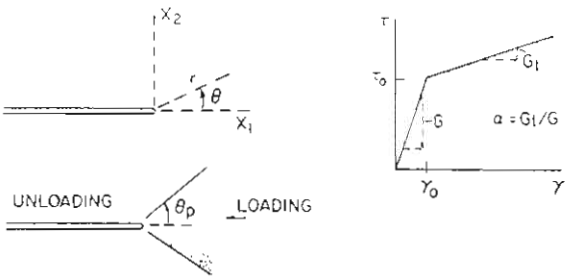

FIG. 1. Crack-tip geometry and stress-strain curve.

Introduce a stress-rate function $\phi(x, y)$, ensuring equilibrium stress-rates, according to

$$\dot{t}_1 = \phi_{,x_2}, \qquad \dot{t}_2 = -\phi_{,x_1}, \tag{2.4}$$

where a subscript comma denotes differentiation with respect to subsequent subscripts. Let $(\dot{t}_r, \dot{t}_\theta)$ and $(\dot{\gamma}_r, \dot{\gamma}_\theta)$ be the components of the stress-rate and strain-rate in the (r, θ) coordinate system of Fig. 1; e.g.

$$\dot{t}_r = \dot{t}_1 \cos\theta + \dot{t}_2 \sin\theta, \qquad \dot{t}_\theta = -\dot{t}_1 \sin\theta + \dot{t}_2 \cos\theta. \tag{2.5}$$

In this system,

$$\dot{t}_r = r^{-1}\phi_{,\theta}, \qquad \dot{t}_\theta = -\phi_{,r}. \tag{2.6}$$

Compatibility of the strain-rates requires

$$(\dot{\gamma}_r)_{,\theta} - (r\dot{\gamma}_\theta)_{,r} = 0. \tag{2.7}$$

After elimination of the strain-rates using (2.2) for plastic loading and (2.6), one obtains for (2.7),

$$\alpha r\nabla^2\phi + (1-\alpha)\{(\tau^{-1}\tau_r\dot{t})_{,\theta} - (r\tau^{-1}\tau_\theta\dot{t})_{,r}\} = 0, \tag{2.8}$$

where (τ_r, τ_θ) are the stress components in the (r, θ) system. In the unloading region,

$$\nabla^2\phi = 0. \tag{2.9}$$

Identify the rate parameter with the increase in crack length so that in a steady state the material derivative and the x_1-gradient of Cartesian components of stress and strain are related by

$$\dot{t}_\beta = -\partial\tau_\beta/\partial x_1, \qquad \dot{\gamma}_\beta = -\partial\gamma_\beta/\partial x_1. \tag{2.10}$$

Equation (2.8) is homogeneous of degree one in the stress-rate function, even taking into account the connection of the stresses to their rates through (2.10). This homogeneity permits us to look for solutions of the form

$$\phi = K\tau_0 r^s f(\theta), \tag{2.11}$$

where K is an amplitude factor, τ_0 is introduced for later convenience and where s and f are to be determined. Symmetry with respect to $\theta = 0$ requires $f(\theta) = f(-\theta)$. This, together with vanishing tractions on $\theta = \pm\pi$, gives the boundary conditions

$$f'(0) = 0, \qquad f(\pi) = 0, \tag{2.12}$$

where a prime denotes differentiation with respect to θ.

We anticipate that plastic loading ($\dot{t} > 0$) will occur for $|\theta| < \theta_p$. The condition for determining the boundary between loading and unloading is

$$\dot{t} = 0, \qquad \theta = \theta_p. \tag{2.13}$$

Elastic unloading with (2.3) is assumed to occur for $|\theta| > \theta_p$. *The possibility of a reversed loading region will not be considered.* CHITALEY and MCCLINTOCK (1971) did find a *secondary* loading zone in their perfectly-plastic analysis, but it extended from $|\theta| = \pi$ by less than half a degree and had *negligible* influence on the rest of the field.

With [ ] denoting the jump in a quantity across θ_p, continuity of traction-rate requires $[\dot{t}_\theta] = 0$. In addition, the displacement-rate $\dot{u}_3$ must be continuous across θ_p which implies that $[\dot{\gamma}_r] = 0$. This, in turn, by (2.3), (2.4) and (2.13), requires $[\dot{t}_r] = 0$. Together the two conditions will be satisfied if and only if

$$[f] \equiv f(\theta_p^+) - f(\theta_p^-) = 0, \qquad [f'] = 0. \tag{2.14}$$

It also follows that $\dot{t}$ is continuous across θ_p.

The following notation is convenient:

$$(\dot{\tau}_\beta, \dot{t}) = K\tau_0 r^{s-1}(t_\beta(\theta), t(\theta)), \tag{2.15}$$

where from (2.4) and (2.6),

$$\left.\begin{aligned} t_r = f', \qquad & t_\theta = -sf, \\ t_1 = s\sin\theta\, f + \cos\theta\, f', \qquad & t_2 = -s\cos\theta\, f + \sin\theta\, f'. \end{aligned}\right\} \tag{2.16}$$

The stress field of the dominant singularity can be written as

$$(\tau_\beta, \tau) = K\tau_0 r^s (T_\beta(\theta), T(\theta)), \tag{2.17}$$

where, from (2.4) and (2.10),

$$T_2 = f \tag{2.18}$$

and

$$\sin\theta\; T_1' = s\cos\theta\; T_1 + t_1. \tag{2.19}$$

Components T_r and T_θ can be expressed in terms of T_1 and T_2 by relations such as (2.5). Note also,

$$T = (T_1^2 + T_2^2)^{\frac{1}{2}} = (T_r^2 + T_\theta^2)^{\frac{1}{2}} \tag{2.20}$$

and

$$t = T^{-1}(T_1 t_1 + T_2 t_2) = T^{-1}(T_r t_r + T_\theta t_\theta). \tag{2.21}$$

All quantities defined above can therefore be expressed in terms of f, f' and T_1. In what follows, f and T_1 will be taken as the basic dependent variables.

The assumed form of the solution is now substituted into (2.8) governing behavior in the loading region. Separating out the most highly differentiated term (i.e. f''), one finds, for $\theta \leq \theta_p$,

$$f''\{\alpha T^2+(1-\alpha)T_r^2\}+\alpha s^2 T^2 f+(1-\alpha)\{-2T'T_r t+TT_r' t+ \\ +T_r(T_r' t_r+T_\theta t_\theta'+T_\theta' t_\theta)-sTT_\theta t\}=0. \qquad (2.22)$$

In the elastic unloading region, the solution to (2.9), which satisfies $f(\pi) = 0$ and continuity of f across θ_p, is

$$f=f(\theta_p^-)\sin(s(\pi-\theta))/\sin(s(\pi-\theta_p)), \qquad \theta \geq \theta_p. \qquad (2.23)$$

Continuity of f' across θ_p, equation (2.14), can be expressed as a condition on f and f' for $\theta \to \theta_p^-$ as

$$f'(\theta_p^-)+s\cot(s(\pi-\theta_p))f(\theta_p^-)=0, \qquad (2.24)$$

where θ_p is unknown *a priori* and must satisfy (2.13), i.e.

$$t(\theta_p)=0. \qquad (2.25)$$

Satisfaction of (2.24) guarantees that the solutions in the loading and unloading regions can be matched across θ_p. Boundary conditions ahead of the crack are

$$f'(0)=0 \qquad (2.26)$$

and the requirement that T_1 be regular at $\theta = 0$; equation (2.26) implies $T_1(0) = T_r(0) = 0$. The θ-variations must be normalized in some manner and the most suitable one for present purposes is $T(0) = T_\theta(0) = 1$, which is equivalent to

$$f(0)=1. \qquad (2.27)$$

Equations (2.19) and (2.22) constitute a homogeneous, third-order system of ordinary differential equations for f and T_1.† It is supplemented by the two homo-

TABLE 1 *Mode III*

α	s	θ_p
1·0	−0·5	1·571
0·7	−0·444	1·523
0·5	−0·394	1·473
0·3	−0·325	1·393
0·2	−0·277	1·329
0·1	−0·207	1·221
0·01	−0·0737	0·907
0·001	−0·0244	0·750

† An alternative formulation can be given in terms of a stress function rather than a stress-rate function. That formulation leads to a single third-order differential equation for the θ-variation of the stress function. We have also solved this equation numerically with the same results reported below. On balance, the formulation reported here is the easiest one to use.

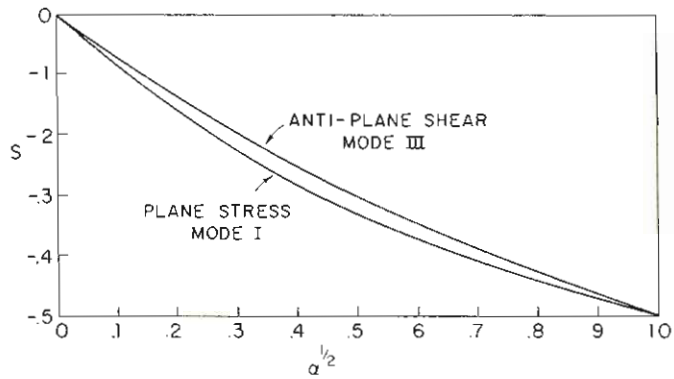

FIG. 2. Order of singularity of stresses and strains.

geneous boundary conditions (2.24) and (2.26), together with the regularity condition at $\theta = 0$, and (2.25) for determining θ_p. The order of the singularity s is the eigenvalue. A discussion of the numerical method is given in the Appendix. In principle, however, the procedure is to specify a trial value of s and then to integrate (2.19) and (2.22) starting at $\theta = 0$ until a value of θ is found at which t vanishes, where condition (2.24) is checked. If (2.24) is satisfied, then the solution has been found; if not, an improved estimate of s is obtained using a procedure discussed in the Appendix and the process is repeated.

Values of s and θ_p for selected values of α ranging over $1 \geq \alpha \geq 0{\cdot}001$ are given in Table 1. In Fig. 2, s is plotted against $\alpha^{\frac{1}{2}}$, since the numerical results so plotted strongly suggest that s is proportional to $\alpha^{\frac{1}{2}}$ for small α. An unsuccessful attempt was made to formulate and solve an asymptotic problem for small α which would reveal explicitly this limiting behavior.

Stress distributions in the loading region are shown in Fig. 3 for $\alpha = 1, 0{\cdot}1, 0{\cdot}01$. With $\alpha = 1$, then $s = -\frac{1}{2}$ and the distributions are identical to those for a stationary crack in a linear elastic material, i.e.

$$f = \cos \tfrac{1}{2}\theta, \qquad T_\theta = \cos \tfrac{1}{2}\theta, \qquad T_r = \sin \tfrac{1}{2}\theta, \qquad T = 1. \tag{2.28}$$

In this limit, t vanishes at $\theta = \frac{1}{2}\pi$, although θ_p is immaterial since the plastic strain-

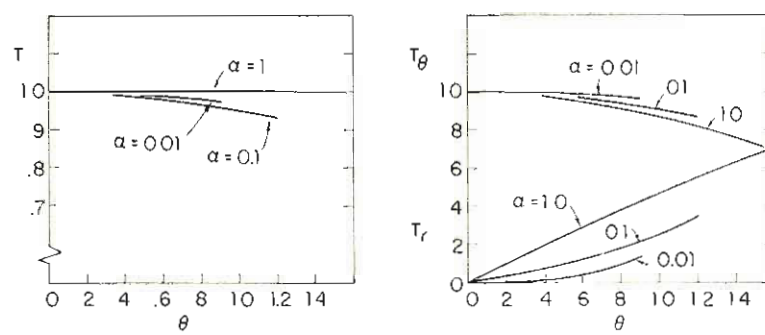

FIG. 3. Stress distributions for $\theta \leq \theta_p$ in anti-plane shear.

rates vanish for all θ. The θ-variations of the stress distribution for low strain-hardening, $\alpha = 0{\cdot}01$ with $s = -0{\cdot}0737$, is seen to be very close to that associated with the slip-line field ahead of an elastic perfectly-plastic crack, i.e.

$$f = \cos\theta, \qquad \tau_\theta = \tau_0, \qquad \tau_r = 0, \qquad \tau = \tau_0. \tag{2.29}$$

The approach to elastic perfectly-plastic behavior is also seen in the plots of the plastic part of the strain-rates in Fig. 4. These can be expressed, using (2.2), (2.15) and (2.17), as

$$\alpha\dot{\gamma}^p_\beta = K\gamma_0 r^{s-1}P_\beta(\theta), \quad \text{with } P_\beta(\theta) = (1-\alpha)T^{-1}T_\beta t, \tag{2.30}$$

where $\gamma_0 = \tau_0/G$. For low strain-hardening ($\alpha = 0{\cdot}01$ in Fig. 4), $P_r \approx 0$, which is consistent with the fact that $P_r = 0$ in an elastic perfectly-plastic slip-line fan at the crack tip.

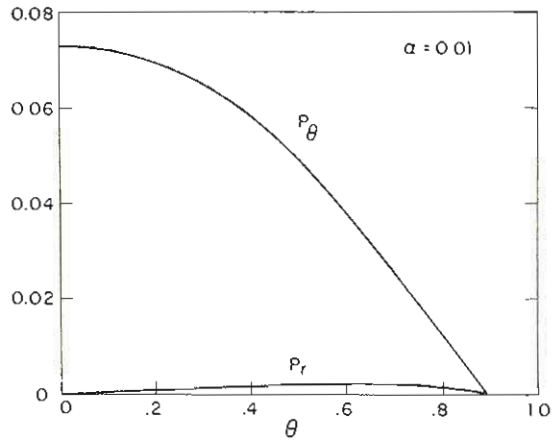

FIG. 4. Plastic strain-rate distribution for low strain-hardening in anti-plane shear (see equation (2.30)).

Directly ahead of the crack, $\theta = 0$, $t = -s$ and $P_\theta = s(1-\alpha)$, this being the largest value of P_θ for $|\theta| \leq \theta_p$. The elastic part of the strain-rate is given by

$$\dot{\gamma}^e_\beta = K\gamma_0 r^{s-1}t_\beta(\theta). \tag{2.31}$$

For low strain-hardening, these components can be estimated quite accurately using (2.16) and (2.29) as

$$\dot{\gamma}^e_r = -K\gamma_0 r^{s-1}\sin\theta, \qquad \dot{\gamma}^e_\theta = -sK\gamma_0 r^{s-1}\cos\theta. \tag{2.32}$$

Thus, directly ahead of the crack the ratio of the elastic strain-rate to the plastic strain-rate is essentially α for low strain-hardening. However, for $\theta \neq 0$, $\dot{\gamma}^e_r$ is the dominant elastic strain-rate component and it is of order α/s compared to the plastic strain-rates. Based on the numerical results for s, this ratio is therefore proportional to $\alpha^{\frac{1}{2}}$ for small α.

3. DISCUSSION OF ANTI-PLANE SHEAR RESULTS

A small amount of strain-hardening has a substantial effect on the crack tip singularity in steady growth in the sense that the strength of the singularity s increases strongly as α increases from zero. A value of α less than $0{\cdot}02$ already gives $s = -0{\cdot}1$.

At the same time, the θ-variations of the stresses and strain-rates are less strongly dependent on variations in small α.

In analogous stationary crack problems, such as those for power-law hardening materials analyzed by HUTCHINSON (1968) and RICE and ROSENGREN (1968), plastic strains dominate elastic strains as the crack tip is approached and elastic strains play no role in the dominant singularity analysis to lowest order. This is *not* the case in the above solutions, *nor* is it true for elastic perfectly-plastic crack growth as discussed by RICE (1973). Elastic strain-rates play an essential role in steady crack-growth behavior and they cannot be neglected in the analysis, even though for small α they are only of order α/s compared to the plastic strain-rates. The singularity fields produced here are *exact* solutions to the field equations involving no approximation, except that (2.2) is taken to hold for all r when $|\theta| \leq \theta_p$, and consequently there is no transition to purely elastic behavior (2.3) when τ falls below τ_0 ahead of the crack.

Passage to the limit of elastic perfect-plasticity is not straightforward. However, as already discussed, the limiting stress field appears to be the slip-line field (2.29) used by CHITALEY and MCCLINTOCK (1971). Using the limiting value of f from (2.29) and taking the limit of (2.24) as $\alpha \to 0$, one finds

$$\cot \theta_p = \pi - \theta_p \Rightarrow \theta_p \approx 19{\cdot}664^\circ. \tag{3.1}$$

This compares with $\theta_p = 19{\cdot}693^\circ$ obtained by Chitaley and McClintock, who take into account the *tiny reversed loading zone* mentioned earlier. We also note that $t = 0$ for all θ in the loading region in the limit $\alpha = 0$ since $\tau = \tau_0$, and thus the side condition (2.25) is also satisfied. On the other hand, numerical results for θ_p in Table 1 are far from (3.1), even for α as small as 10^{-3}, although θ_p is still decreasing strongly even at these small values of α. One cannot conclude from our numerical results whether or not θ_p approaches (3.1) in the limit. *The important conclusion to be drawn is that θ_p is significantly affected by strain-hardening.*

It is not possible to let $\alpha \to 0$ in the expression for the plastic strain-rates (2.30). This is to be expected since the amplitude of the plastic strain-rates is not tied to the near-tip stress field for perfect-plasticity. For $\alpha > 0$, stress-rates and strain-rates are uniquely related and the equations are *elliptic*; but for $\alpha = 0$ the equations become *hyperbolic* and the unique relationship breaks down.

SLEPYAN (1973) has considered a problem which is similar to the present one in all respects except, instead of J_2 flow theory, he uses J_2 deformation theory in the loading region. He is able to arrive at a closed-form expression relating s to θ_p. Because of the inherent lack of continuity of the strain-rate when deformation theory is coupled with elastic unloading, θ_p is not uniquely determined in his analysis. Slepyan chooses θ_p to give the strongest possible singularity which leads to results very close to the present ones in Fig. 2. Flow theory with a smooth yield surface, such as that used here, gives rise to an effective incremental stiffness which is most likely larger than that of an actual metal for the non-proportional stress histories involved in crack growth. In contrast, deformation theory probably underestimates the effective incremental stiffness. Thus, it is notable that the two calculations give comparable results for s as a function of α.

4. PLANE STRESS ANALYSIS

Here σ_0 denotes the yield stress in tension and $\varepsilon_0 = \sigma_0/E$ is the yield strain, where E is Young's modulus. Let E_t denote the slope of the bilinear stress–strain relation in tension for stresses in excess of σ_0 and now take $\alpha = E_t/E$. With s_{ij} as the stress deviator and $\sigma_e = (\frac{3}{2}s_{ij}s_{ij})^{\frac{1}{2}}$ as the effective stress, the constitutive relation according to J_2 flow theory for an elastically isotropic solid is

$$E_t\dot{\varepsilon}_{ij} = \begin{cases} \alpha[(1+\nu)\dot{\sigma}_{ij} - \nu\dot{\sigma}_{kk}\delta_{ij}] + (3/2\sigma_e)(1-\alpha)s_{ij}\dot{\sigma}_e & \text{(loading, } \dot{\sigma}_e \geq 0), \quad (4.1) \\ \alpha[(1+\nu)\dot{\sigma}_{ij} - \nu\dot{\sigma}_{kk}\delta_{ij}] & \text{(unloading, } \dot{\sigma}_e < 0), \quad (4.2) \end{cases}$$

where ν is Poisson's ratio.

With $\dot{\sigma}_{rr}$, $\dot{\sigma}_{\theta\theta}$, $\dot{\sigma}_{r\theta}$ denoting components of the stress-rate in an (r, θ) coordinate system centered at the crack tip, equilibrium is satisfied by introduction of a stress-rate function according to

$$\dot{\sigma}_{rr} = r^{-1}\phi_{,r} + r^{-2}\phi_{,\theta\theta}, \qquad \dot{\sigma}_{\theta\theta} = \phi_{,rr}, \qquad \dot{\sigma}_{r\theta} = -(r^{-1}\phi_{,\theta})_{,r}. \tag{4.3}$$

Compatibility of the in-plane strain-rates requires

$$r^{-1}(r\dot{\varepsilon}_{\theta\theta})_{,rr} + r^{-2}\dot{\varepsilon}_{rr,\theta\theta} - r^{-1}\dot{\varepsilon}_{rr,r} - 2r^{-2}(\dot{\varepsilon}_{r\theta,\theta}r)_{,r} = 0, \tag{4.4}$$

where the strain-rate components in (4.4) are those in the (r, θ) system.

In plane stress, the stress components σ_{33}, σ_{13}, σ_{23} are taken to be zero. Under this assumption, (4.4) becomes, on eliminating the strain-rates using (4.1) or (4.2) and (4.3),

$$\alpha\nabla^4\phi + \tfrac{3}{2}(1-\alpha)\{r^{-1}(r\sigma_e^{-1}s_{\theta\theta}\dot{\sigma}_e)_{,rr} + r^{-2}(\sigma_e^{-1}s_{rr}\dot{\sigma}_e)_{,\theta\theta} - r^{-1}(\sigma_e^{-1}s_{rr}\dot{\sigma}_e)_{,r} - 2r^{-2}[r(\sigma_e^{-1}\sigma_{r\theta}\dot{\sigma}_e)_{,\theta}]_{,r}\} = 0 \quad \text{for } \dot{\sigma}_e \geq 0, \tag{4.5}$$

$$\nabla^4\phi = 0 \quad \text{for } \dot{\sigma}_e < 0. \tag{4.6}$$

Cartesian components of stress and strain are connected to their corresponding rates by steady-state relations analogous to (2.10):

$$\dot{\sigma}_{ij} = -\sigma_{ij,x_1}, \qquad \dot{\varepsilon}_{ij} = -\varepsilon_{ij,x_1}. \tag{4.7}$$

Here, solutions are sought of the form

$$\phi = K\sigma_0 r^{s+1}f(\theta), \tag{4.8}$$

$$(\dot{\sigma}_{ij}, \dot{\sigma}_e) = K\sigma_0 r^{s-1}(t_{ij}(\theta), t(\theta)), \tag{4.9}$$

$$(\sigma_{ij}, \sigma_e, s_{ij}) = K\sigma_0 r^s(\Sigma_{ij}(\theta), \Sigma(\theta), S_{ij}(\theta)), \tag{4.10}$$

where s is anticipated to be in the range $-\frac{1}{2} \leq s \leq 0$. From (4.3),

$$t_{rr} = (s+1)f + f'', \qquad t_{\theta\theta} = s(s+1)f, \qquad t_{r\theta} = -sf'. \tag{4.11}$$

From (4.7),

$$\Sigma_{22} = -(s+1)\cos\theta\ f + \sin\theta\ f', \qquad \Sigma_{12} = (s+1)\sin\theta\ f + \cos\theta\ f' \tag{4.12}$$

and

$$\sin\theta\ \Sigma_{11}' = s\cos\theta\ \Sigma_{11} + t_{11}, \tag{4.13}$$

where t_{11} can be expressed in terms of t_{rr}, $t_{\theta\theta}$, $t_{r\theta}$ using standard formulae for changes in components under rotation of axes. Also,

$$\Sigma = (\tfrac{3}{2}S_{ij}S_{ij})^{\frac{1}{2}}, \qquad t = \tfrac{3}{2}\Sigma^{-1}S_{ij}^{*}t_{ij}. \tag{4.14}$$

Reduction of (4.5) governing behavior in the loading region ($\dot{\sigma}_e \geq 0$, $\theta \leq \theta_p$) is lengthy, but straightforward, and will not be given here.† The result can be expressed in the form

$$f^{iv} = F(\alpha, s, \theta, f, f', f'', f''', \Sigma_{11}) \quad \text{for } \theta \leq \theta_p. \tag{4.15}$$

Equations (4.13) and (4.15) comprise a 5th-order system. Equation (4.15) emphasizes that f^{iv} is determined if the arguments of F indicated are specified (ν does not enter); for numerical work it does not pay explicitly to eliminate quantities such as t_{ij} and Σ_{ij}. *The possibility of a secondary loading region is excluded from consideration.* In the elastic unloading region, the solution to (4.6) is

$$f = b_1[(s+1)\sin((s-1)(\pi-\theta)) - (s-1)\sin((s+1)(\pi-\theta))] + \\ + b_2[\cos((s-1)(\pi-\theta)) - \cos((s+1)(\pi-\theta))], \qquad \theta > \theta_p, \tag{4.16}$$

where b_1 and b_2 are undetermined constants and f satisfies traction-free conditions at $\theta = \pi$, i.e. $f = f' = 0$.

The boundary between loading and elastic unloading is determined by $\dot{\sigma}_e = 0$, i.e.

$$t(\theta_p) = 0. \tag{4.17}$$

Continuity of traction-rates across θ_p requires

$$[f] = [f'] = 0, \tag{4.18}$$

and these conditions can be used to solve for b_1 and b_2 in terms of $f(\theta_p^-)$ and $f'(\theta_p^-)$. Continuity of the r-component of the displacement-rate implies that $\dot{\varepsilon}_{rr}$ is continuous across θ_p. This, together with (4.1), (4.2) and (4.17), implies that $\dot{\sigma}_{rr}$ is continuous across θ_p, which requires

$$[f''] = 0. \tag{4.19}$$

It also follows that $\dot{\sigma}_e$ is continuous across θ_p. The relation

$$(r\dot{\varepsilon}_{r\theta})_{,r} - \dot{\varepsilon}_{rr,\theta} = r\dot{u}_{\theta,rr} \tag{4.20}$$

reveals that $[(r\dot{\varepsilon}_{r\theta})_{,r} - \dot{\varepsilon}_{rr,\theta}]$ must be continuous across θ_p. From (4.1), (4.2) and the continuity of f and its first two derivatives, this condition is equivalent to

$$\alpha[f'''] - \tfrac{3}{2}(1-\alpha)\Sigma^{-1}S_{rr}t'\big|_{\theta=\theta_p^-} = 0. \tag{4.21}$$

Ahead of the crack, symmetry associated with Mode I requires

$$f' = f''' = 0, \qquad \theta = 0, \tag{4.22}$$

and in addition f is required to be regular at $\theta = 0$. To normalize the θ-variations, we take

$$\Sigma(0) = 1. \tag{4.23}$$

The numerical procedure is similar to that for anti-plane shear except that now there are two unknown parameters s and q, where

$$q = \Sigma_{11}(0)/\Sigma_{22}(0). \tag{4.24}$$

† No terms are neglected in this reduction, as was also the case in anti-plane shear. As a double check on the results presented for plane stress, and for plane strain given later, each of the present writers has *independently* derived all equations. Furthermore, each writer has *independently* calculated most of the numerical results presented in the present paper.

For a given α, with s and q prescribed, f is determined from (4.15) with an estimate of θ_p from (4.17). At this θ_p, a check is made on whether or not the two jump conditions, equations (4.19) and (4.21), are satisfied. If not, new estimates of s and q are obtained using Newton's method and the process is repeated until satisfactory convergence is obtained.

TABLE 2. *Plane stress*

α	s	θ_p
1·0	−0·5	1·398
0·75	−0·468	1·410
0·25	−0·335	1·371
0·1	−0·237	1·285
0·05	−0·178	1·214
0·01	−0·0864	1·066
0·005	−0·0624	1·017

Selected values of s and θ_p are given in Table 2 and a plot of s against $\alpha^{\frac{1}{2}}$ can be compared with the corresponding curve for anti-plane shear in Fig. 2. Stress distributions in the loading region are shown as solid-line curves in Fig. 5 for the

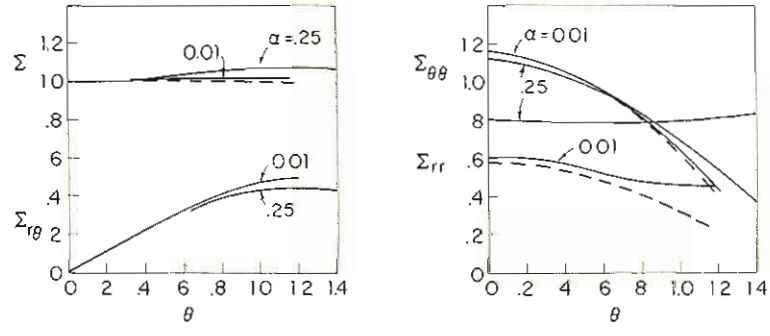

FIG. 5. Stress distributions for $\theta \leqslant \theta_p$ in plane stress. Dashed curves from perfectly-plastic slip-line field, equations (4.25).

cases $\alpha = 0{\cdot}25$, $0{\cdot}01$. Also shown, as dashed-line curves, are stress components associated with the slip-line field of an elastic perfectly-plastic solution for a crack in plane stress. In the loading region ahead of the crack, this solution is (HUTCHINSON, 1968)

$$\sigma_{\theta\theta} = 2\sigma_{rr} = \frac{2}{\sqrt{3}}\,\sigma_0 \cos\theta, \qquad \sigma_{r\theta} = \frac{1}{\sqrt{3}}\,\sigma_0 \sin\theta. \tag{4.25}$$

The θ-variations for low strain-hardening ($\alpha = 0{\cdot}01$) are very close to those given by (4.25). (Dashed curves for $\Sigma_{\theta\theta}$ and $\Sigma_{r\theta}$ are not shown in Fig. 5 since they are indistinguishable for $\alpha = 0{\cdot}01$.)

Further evidence that the solution is approaching the slip-line field for perfect-plasticity can be seen in Fig. 6, where plots are shown of θ-variations of the plastic

strain-rate defined by

$$\alpha\dot{\varepsilon}^{p}_{ij} = K\varepsilon_0 r^{s-1} P_{ij}(\theta). \tag{4.26}$$

Note that $P_{rr}(\theta)$ is very small compared to the other two components. This is consistent with $s_{rr} = 0$ according to (4.25), so that for perfect-plasticity $\dot{\varepsilon}^{p}_{rr} = 0$.

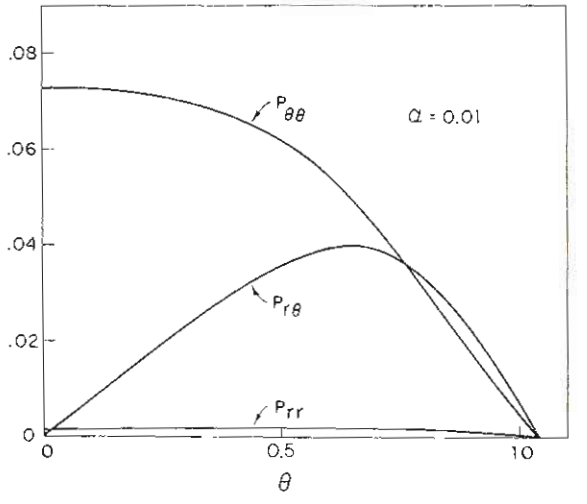

FIG. 6. Plastic strain-rate distribution for low strain-hardening in plane stress (see equation (4.26)).

5. PLANE STRAIN ANALYSIS

The constitutive relation is still (4.1) and (4.2). The plane strain condition $\dot{\varepsilon}_{33} = 0$ gives

$$\dot{\sigma}_{33} = [\alpha + \tfrac{9}{4}(1-\alpha)s^2_{33}\sigma_e^{-2}]^{-1}[\alpha\nu(\dot{\sigma}_{\theta\theta}+\dot{\sigma}_{rr}) - \\ -\tfrac{9}{4}(1-\alpha)s_{33}\sigma_e^{-2}(s_{rr}\dot{\sigma}_{rr}+s_{00}\dot{\sigma}_{\theta\theta}+2\sigma_{r\theta}\dot{\sigma}_{r\theta})] \tag{5.1}$$

which expresses $\dot{\sigma}_{33}$ in terms of the in-plane stress-rates. Equations (4.3), (4.4), (4.6) and (4.7) continue to hold, while the terms

$$-\nu\alpha[r^{-1}(r\dot{\sigma}_{33})_{,rr} - r^{-1}\dot{\sigma}_{33,r} + r^{-2}\dot{\sigma}_{33,\theta\theta}] \tag{5.2}$$

must be added to the left side of (4.5). The form of the dominant singularity is again (4.8)–(4.10); and (4.11)–(4.14) still hold, although now σ_{33} must be included in s_{ij} and Σ.

The governing equation for f is of the same general form (4.15) as in plane stress, except that it is more lengthy and depends on Poisson's ratio ν. Equation (4.16) governing behavior in the elastic unloading regime still pertains as does (4.17). Continuity conditions across θ_p continue to be governed by (4.18) and (4.19), but (4.20) becomes

$$\alpha(1-\nu^2)[f''']^- - \tfrac{3}{2}(1-\alpha)\Sigma^{-1}(S_{rr}+\nu S_{33})t'\big|_{\theta=\theta_p^-} = 0. \tag{5.3}$$

At $\theta = 0$, equation (4.22) applies. In plane strain, the normalization (4.23) is no

longer convenient since $\Sigma(0)$ turns out to be small compared to $\Sigma(\theta_p)$. Instead, take

$$\max \{\Sigma(\theta), |\theta| \leq \theta_p\} = 1. \tag{5.4}$$

The numerical scheme is similar to that previously outlined for plane stress and discussed in the Appendix.

TABLE 3. *Plane strain*

$\alpha\ (\nu = \frac{1}{3})$	s	θ_p	$\alpha\ (\nu = \frac{1}{2})$	s	θ_p
1	−0·5	1·548	1	−0·5	1·571
0·5	−0·442	1·717	0·5	−0·436	1·756
0·3	−0·373	1·875	0·3	−0·356	1·899
0·1	−0·197	2·174	0·1	−0·180	2·186
0·05	−0·136	2·393	0·05	−0·129	2·413
0·01	−0·0887	2·736	0·01	−0·0865	2·762

Numerical values of s and θ_p are given in Table 3 for $\nu = \frac{1}{3}$ and $\frac{1}{2}$, and curves of s as a function of $\alpha^{\frac{1}{2}}$ are given in Fig. 7. The dependence of s on ν is not strong, nor do the θ-variations depend significantly on ν. The dependence of s on α is similar to that in anti-plane shear and plane stress, but it does not appear that s is proportional to $\alpha^{\frac{1}{2}}$ for small α.

Curves of $\Sigma(\theta)$ in the loading region are shown in Fig. 8, where it can be seen that the maximum value of Σ is attained at θ_p. For low strain-hardening, $\alpha = 0{\cdot}01$, the loading zone extends to $\theta_p = 157°$. Stress distributions are shown in Fig. 9 for $\alpha = 1$ (the elastic solution) and $\alpha = 0{\cdot}01$. The results in Fig. 9 are for $\nu = \frac{1}{3}$; the in-plane stresses are imperceptibly different for those for $\nu = \frac{1}{2}$. For low strain-hardening, high triaxial stressing occurs ahead of the crack (with $\Sigma_{33} \approx \frac{1}{2}(\Sigma_{rr} + \Sigma_{\theta\theta})$), just as for the stationary crack in plane strain, Mode I. However, even with as little strain-hardening as $\alpha = 0{\cdot}01$, the stress distribution is still distinct from the well-known Prandtl–Hill slip-line field at the tip of a stationary crack in an elastic perfectly-plastic material, although it may be tending toward that limit as $\alpha \to 0$. (For example,

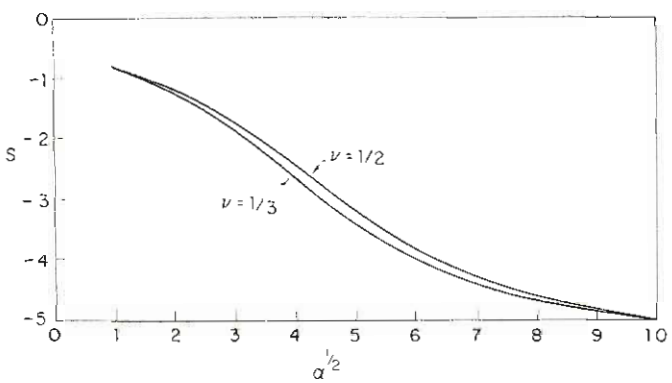

FIG. 7. Order of singularity of stresses and strains for plane strain.

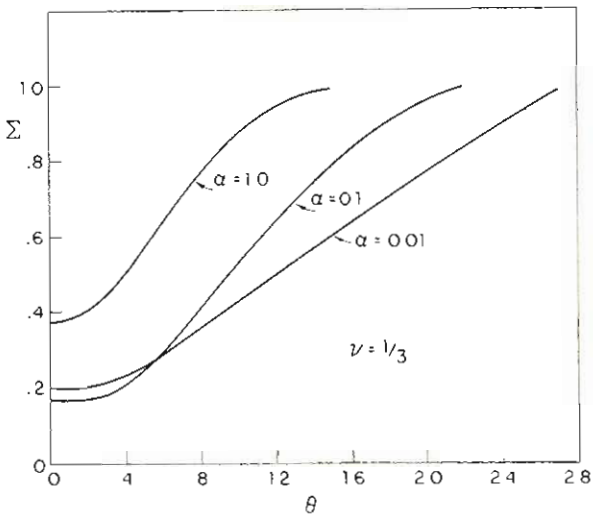

FIG. 8. Effective stress distributions in plane strain.

for the stationary crack with $\alpha = 0$, $\Sigma_{\theta\theta}(0) \approx 2{\cdot}9$ and $\Sigma_{rr}(0) \approx 1{\cdot}8$ with the present normalization. Figure 9 can be compared with HUTCHINSON (1968, Figure 5).) In this respect, plane strain growth seems to be different from anti-plane shear and plane stress discussed above. This is not altogether unexpected. The perfect-plasticity slip-line fans in anti-plane shear and in plane stress lie ahead of the crack and the stress distributions in the fans are fully determined by symmetry and equilibrium, independent of boundary conditions at $\theta = \pm\pi$. In the stationary plane strain problem, a slip-line fan lies above (and below) the crack in the region $\pi/4 \leq \theta \leq 3\pi/4$, and stresses ahead of the crack do depend on the boundary conditions at $\theta = \pm\pi$ behind the crack. Thus, it is not surprising that elastic unloading in the growing crack

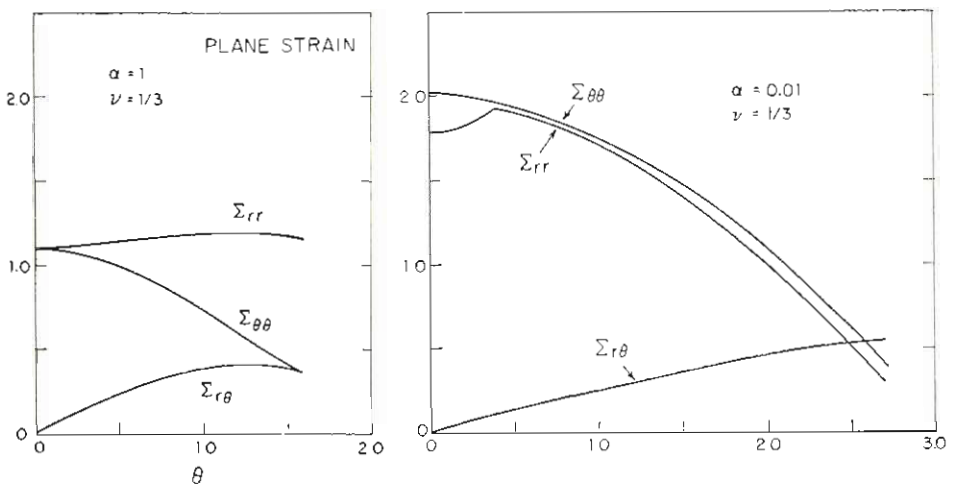

FIG. 9. Stress distributions for $\theta \leq \theta_p$ in plane strain.

problem has more influence on the stresses ahead of the crack in plane strain than in the other two cases.

Components of the plastic strain-rate (4.26) are shown in Fig. 10 for the low strain-hardening case $\alpha = 0{\cdot}01$. The predominant component is $\dot{\varepsilon}^p_{r\theta}$. Ahead of the crack, the plastic strain-rates are relatively small, although not negligible. Starting at $\theta \approx 20°$, $\dot{\varepsilon}^p_{r\theta}$ becomes substantial, extending back to $\theta_p \approx 150°$. By comparison, plastic strains extend only from $\theta = 45°$ to $\theta = 135°$ in the stationary problem. (See, for example, the strain distributions given by HUTCHINSON (1968) for a low strain-hardening power-law material.)

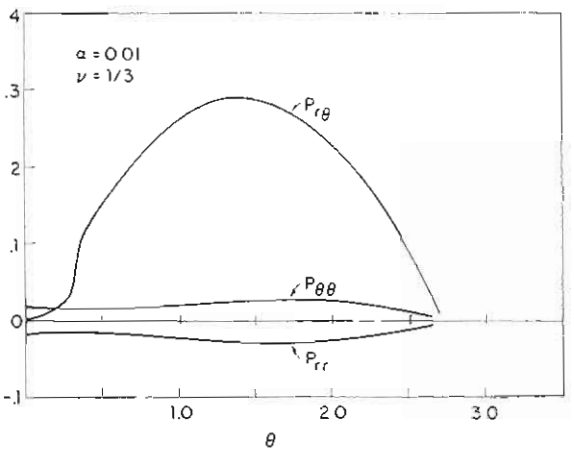

FIG. 10. Plastic strain-rate distribution for low strain-hardening in plane strain (see equation (4.26)).

6. DISCUSSION

A *moderate* amount of strain-hardening gives rise to a fairly *robust* singularity. The amplitude factor K provides a unique measure of the intensity of the singularity fields, and it is through K that the overall geometry and the loading make their presence felt at the tip. *The determination of* K *is a separate problem in itself and it has not been addressed here.*

Even with strain-hardening, the singularity in the strains is not nearly as strong as in the stationary problem. This is the main source of crack growth stabilization, as first shown by MCCLINTOCK (1958) and as discussed further by RICE (1968, p. 277). For example, for an elastic perfectly-plastic material with a stationary crack, the strains vary like r^{-1} as the tip is approached. According to the present steady-growth analysis, the corresponding variation is r^s, where s is typically on the order of $-0{\cdot}2$ for moderate strain-hardening. (The limit $\alpha \to 0$ leads to a logarithmic variation in r for the strains since the strain-rates are then proportional to r^{-1}, as noted in previous work.)

For low to moderate strain-hardening in anti-plane shear and plane stress, the θ-variations of the stress fields ahead of the crack are not significantly different from those for the corresponding stationary crack in an elastic perfectly-plastic material. However, in plane strain two new features have emerged. First, the level of triaxial

stress ahead of the crack may not be as intense as in the stationary case. Secondly, there appears to be a redistribution of the crack-tip strain-rates, and therefore strains, towards the forward part of the field. The first effect would be expected to have a stabilizing influence, while the latter would probably have the opposite effect.

References

Chitaley, A. D. and McClintock, F. A.	1971	*J. Mech. Phys. Solids* **19**, 147.
Hutchinson, J. W.	1968	*Ibid.* **16**, 337.
McClintock, F. A.	1958	Trans. ASME, Ser. *E*, **80**, *J. appl. Mech.* **25**, 582.
Rice, J. R.	1968	*Fracture: An Advanced Treatise* (edited by Liebowitz, H.), Vol. 2: *Mathematical Fundamentals*, Ch. 3, pp. 191–311. Academic Press, New York.
	1973	*Mechanics and Mechanisms of Crack Growth*, (Proceedings of Conference at Churchill College, Cambridge, April 1973), (edited by May, M. J.), pp. 14–39. British Steel Corporation, Physical Metallurgy Centre, Swinden Laboratories, Moorgate, Rotherham.
Rice, J. R. and Rosengren, G.	1968	*J. Mech. Phys. Solids* **16**, 1.
Slepyan, L. I.	1973	*Izv. Akad. Nauk. SSSR. Mekhanika Tverdogo Tela* **8**, 139. (Translated from the Russian.)

Appendix

Numerical Analysis

1. *Anti-plane shear*

To integrate forward using (2.22) and (2.19) with $f(0) = 1$, $f'(0) = 0$ and T_1 regular at $\theta = 0$, we start the solution using Taylor series expansions about $\theta = 0$:

$$\left.\begin{aligned} f &= 1+\tfrac{1}{2}a\theta^2+\tfrac{1}{24}b\theta^4+\ldots,\\ f' &= a\theta+\tfrac{1}{6}b\theta^3+\ldots,\\ T_1 &= \lambda\theta+\mu\theta^3+\ldots. \end{aligned}\right\} \tag{A.1}$$

Direct substitution into (2.19) and (2.22) gives

$$\left.\begin{aligned} a &= s(s^2-s+1-\alpha)/(\alpha-s),\\ \lambda &= (a+s)/(1-s),\\ \mu &= (b-2s\lambda-2a+3as)/[6(3-s)], \end{aligned}\right\} \tag{A.2}$$

together with a more lengthy expression for b which will not be shown. This expansion provided values of f and T_1 at $\theta = \Delta\theta$, where $\Delta\theta$ is the integration step-size. From this point on, the integration was carried out numerically according to the following prescription.

Let f_i, f_i' and T_{1i} be known values at $\theta = i\Delta\theta$. Then, f_i'' and T_{1i}' may be calculated from (2.22) and (2.19). To calculate values at $\theta = (i+1)\Delta\theta$, an implicit integration

scheme was used, where

$$\left.\begin{aligned} f_{i+1} &= f_i + f_i'\Delta\theta + \tfrac{1}{2}f_i''(\Delta\theta)^2 + \tfrac{1}{6}c(\Delta\theta)^3, \\ f_{i+1}' &= f_i' + f_i''\Delta\theta + \tfrac{1}{2}c(\Delta\theta)^2, \\ T_{1i+1} &= T_{1i} + T_{1i}'\Delta\theta + \tfrac{1}{2}T_{1i}''(\Delta\theta)^2 + \tfrac{1}{6}T_{1i}'''(\Delta\theta)^3. \end{aligned}\right\} \tag{A.3}$$

Here, c is chosen, by straightforward numerical iteration, so that

$$f_{i+1}'' \equiv f_i'' + c\Delta\theta$$

equals f'' at $\theta = (i+1)\Delta\theta$ calculated from (2.22) using f_{i+1}, f_{i+1}' and T_{1i+1} given by the above formulae. Note that T_{1i}'' and T_{1i}''' can be determined from derivatives of (2.19) as

$$\left.\begin{aligned} T_{1i}'' &= -(\sin\theta)^{-2}(sT_{1i} + f_i') + \cot\theta\,(sT_{1i}' + f_i'') + sf_i', \\ T_{1i}''' &= 2(\sin\theta)^{-2}\cot\theta\,(sT_{1i} + f_i') - 2(\sin\theta)^{-2}(sT_{1i}' + f_i'') + \cot\theta\,(sT_{1i}'' + c) + sf_i''. \end{aligned}\right\} \tag{A.4}$$

With a typical step-size of $\Delta = 0{\cdot}01$ rad, the above scheme was found to be accurate, efficient and stable.

As discussed in the text of the present paper, the integration is carried forward until a value $\theta = \theta_p$ is found where $t = 0$. At this value of θ, the left side of (2.24) is evaluated. The whole process is then repeated with a slightly different value of s. These two results can then be used to obtain an improved estimate of s for which (2.24) will be satisfied. The entire process is repeated until satisfactory convergence of s is obtained. By varying the step-size $\Delta\theta$, we have obtained some insight into the accuracy of s and θ_p. The valueis n Table 1 appear to be accurate to at least three significant figures.

2. *Plane stress and plane strain*

The numerical method used for the two plane cases is analogous to that for anti-plane shear. Now, however, there are two unknown parameters, s and q, which must be iterated and two conditions at θ_p which must be satisfied, equations (4.19) and (4.21) or (5.3). This is accomplished using Newton's method. Let d denote the left side of (4.19) and e denote the left side of (4.21) or (5.3) for given values of s and q. Let $s+\Delta s$ and $q+\Delta q$ be improved estimates. According to Newton's method, Δs and Δq should be chosen to satisfy the simultaneous equations

$$d + \frac{\partial d}{\partial s}\Delta s + \frac{\partial d}{\partial q}\Delta q = 0, \qquad e + \frac{\partial e}{\partial s}\Delta s + \frac{\partial e}{\partial q}\Delta q = 0. \tag{A.5}$$

The partial derivatives in (A.5) were evaluated numerically using approximate formulae such as

$$\frac{\partial d}{\partial s} \approx \frac{1}{\varepsilon}[d(s+\varepsilon, e) - d(s, e)], \tag{A.6}$$

where ε is chosen sufficiently small compared to s.

Integration of (4.15) is again started using a Taylor series about $\theta = 0$ which is correct up to and including terms of order θ^4 in f and order θ^3 in Σ_{11}. The integration formula for f_{i+1} is now

$$f_{i+1} = f_i + f_i'\Delta\theta + \frac{1}{2!}f_i''(\Delta\theta)^2 + \frac{1}{3!}f_i'''(\Delta\theta)^3 + \frac{1}{4!}f_i^{iv}(\Delta\theta)^4 + \frac{1}{5!}c(\Delta\theta)^5 \tag{A.7}$$

with expressions which follow directly for f'_{i+1}, *etc.* In this expression f_i^{iv} is calculated from (4.15) and c is found numerically such that $f_i^{iv} + c\Delta\theta$ equals f^{iv} evaluated using (4.15) at $\theta = (i+1)\Delta\theta$, in analogy to the implicit scheme used in anti-plane shear.

Of the three cases, plane strain placed the most severe test on the numerical method. For low strain-hardening, the higher derivatives of f become very large in the neighborhood of $\theta = 0{\cdot}4$, as can be inferred from the plot of $P_{r\theta}$ in Fig. 10.